Progress In Electromagnetics Research M, Vol. 61, 51–60, 2017

A Study of Scattering from Snow Embedded with Non-Spherical Shapes of Scatterers with Relaxed Hierarchical Equivalent Source Algorithm (RHESA)

Chan-Fai Lum[1], Fu Xin[2], Hong-Tat Ewe[1, *], and Li-Jun Jiang[2]

Abstract—Remote sensing has been used widely in studying the earth terrain such as snow or sea ice due to its fast, convenient and long-term monitoring capabilities. SAR images acquired could be used to analyze the condition of snow, snow water equivalent (SWE), surface roughness and others. Theoretical models have also been developed to understand how microwave interacts with the snow medium and the scatterers embedded inside the medium. Conventionally, spherical shape of scatterers is commonly used to represent the ice particles embedded inside snow where the actual shape of scatterers can vary. This paper is to present a theoretical model based on radiative transfer formulation that utilizes computational electromagnetics in the modelling of scattering from arbitrary shape of scatterers. The paper also studies the effect of scatterer shape on scattering mechanisms and total backscattering coefficient. Numerical solution of Relaxed Hierarchical Equivalent Source Algorithm (RHESA) was integrated with existing radiative transfer theoretical model to simulate a layer of random discrete snow medium. Several shapes of scatterers were simulated, and theoretical simulation were compared with ground truth measurement data with promising results.

1. INTRODUCTION

Traditionally, Radiative Transfer (RT) theory can be used to study the propagation of microwave through random discrete medium. RT theoretical models have been developed and used to simulate major types of mediums such as snow, sea ice and vegetation [1–6]. For densely packed medium, two popular methods were developed which are quasicrystalline approximation (QCA) [7] and phase and amplitude correction theory [8]. Due to the difficulty in deriving formulations for different shapes of scatterers, basic shapes of scatterers like cylinder, sphere, disk or ellipsoid were commonly used to represent the ice particles or brine inclusions [1–4] or trunk, branches or leaves of vegetation [4–6]. Despite the difficulty, there were studies on nonspherical particles performed by previous researchers since 1984 [9]. New improved RT theoretical model that can better represent the scatterers inside the medium could help researchers to better model the earth terrain and understand the scattering mechanisms.

The spherical shape of scatterers is commonly used in existing RT theoretical model for the modelling of snow medium. To find the total backscattering coefficient, scattering from these spherical scatterers was calculated using Mie-scattering formulation [3]. In the modeling configuration, there are three layers which consist of air layer as top layer, snow layer as middle layer and either soil or sea ice as the lower layer. The boundary between air layer and snow layer is modelled as a top rough surface, and the boundary between the snow layer and lower layer is modelled as a bottom rough surface. Scattering

Received 5 May 2017, Accepted 30 September 2017, Scheduled 10 October 2017

* Corresponding author: Hong-Tat Ewe (eweht@utar.edu.my).

[1] Lee Kong Chian Faculty of Engineering and Science, Universiti Tunku Abdul Rahman, Sungai Long, Malaysia. [2] Department of Electronic and Electrical Engineering, The University of Hong Kong Pokfulam, Hong Kong, China.

from these two rough surfaces were computed using integral-equation-based surface scattering model (IEM) [10] model.

Analytical solution to simulate certain shape of scatterers has limited the existing RT theoretical model to be further used in research works that involve different kinds of snow or ice layers such as snow ice, frazil ice and columnar ice where scatterers inside are in granular or tubular form [11]. Research works [12, 13] show that the shape of scatterers could have significant contribution on total backscattering coefficient. The study shows that snow medium could have different shapes of scatterers instead of just spherical scatterers. This is because metamorphism process can alter the ice grain shape due to the heat flow and pressure change [14, 15].

Incorporating numerical solution with existing RT theoretical model can allow the new improved RT theoretical model to simulate different shapes of scatterers without the need to derive analytical formulations when a new shape is considered. This provides great convenience for model simulation as the formulation could be difficult and time consuming especially for irregular shape of scatterers. In recent years, computational electromagnetics (CEM) has become important and gained a lot of interest in modern engineering and science fields. The emergence and use of Method of Moments (MoM) [16] allow the electromagnetics integral equations to be converted into a matrix-form linear equations that a powerful computer can solve it approximately. More and more numerical algorithms have been successfully applied with MoM and the computational speed has been improved through methods such as equivalence principle algorithm (EPA) [17, 18], relaxed hierarchical equivalent source algorithm (RHESA) [19], multilevel fast multipole algorithm (MLFMA) [20] and finite-difference time-domain method (FDTDM) [21]. With more powerful computers, solving scattering problems with CEM is a direction that the existing RT theoretical model could move on.

RHESA is a newly implemented numerical solution based on EPA foundation. In EPA, the original sources are replaced by electric and magnetic currents on an equivalence surface and these are known as equivalent source. EPA can reduce the unknowns and decompose one whole solution into several subproblems based on domain decomposition method (DDM) [17]. To eliminate the problem of singularities faced in EPA, RHESA uses relaxed hierarchical arrangement of spherical equivalence surfaces to avoid interception with internal primary sources. RHESA can reduce the total unknowns and accelerate the computational speed by utilizing the hierarchical form of equivalent sources that act as intermediate sources to compute the far-field interactions [19].

2. MODEL DESCRIPTION AND METHODOLOGY

As shown in Figure 1, the form of ice particles can be different due to the metamorphism and sintering process [14, 15]. In this section, a new improved RT theoretical model is presented to give the capability to simulate non-spherical shape of scatterers. The RT theoretical model is developed for densely packed medium which includes the array phase and amplitude correction theory. The theory has taken into account the near-field interactions between scatterers by applying a modified phase matrix which takes in the near-field term of the scattered field of the scatterers and coherent effect of the scatterers by multiplying Stokes matrix of a single scatterer with a phase correction factor. The array phase correction

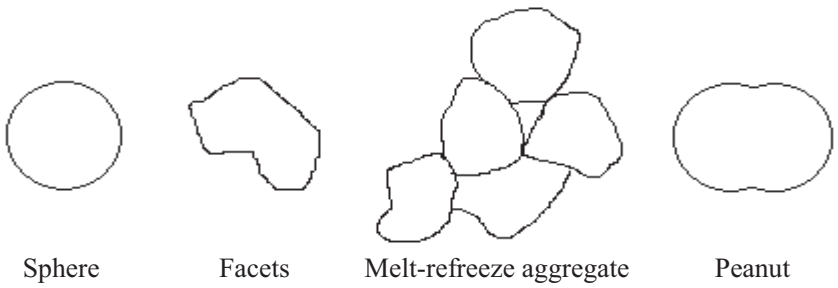

Figure 1. Some of the forms of ice particles that change due to the metamorphism and sintering process.

factor was developed based on antenna array theory. Volume fraction is used to describe the density of scatterer per unit volume, and the average distance between scatterers is given by $d = (V_o/V_f)^{1/3}$ where V_o is the volume of the scatterer, and V_f is the volume fraction.

Figure 2 shows the model configuration for a layer of snow with identical spherical scatterers embedded inside with top and bottom rough surfaces. The lower half or layer beneath can be ground or sea ice.

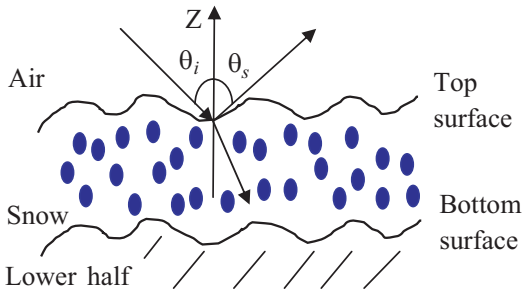

Figure 2. Illustration of model configuration for a layer of snow with spherical scatterers.

Generally, the total backscattering coefficient from the medium can be given by summing up backscattering components from surface scattering, surface-volume scattering and volume scattering [2] as shown in Equation (1):

$$\sigma_{pq}^{\text{total}} = \sigma_{pq}^{\text{surface}} + \sigma_{pq}^{\text{surface-volume}} + \sigma_{pq}^{\text{volume}} \tag{1}$$

This is obtained by solving the radiative transfer equation [1] iteratively up to second order. The radiative transfer equation used is shown in Equation (2):

$$\cos\theta \frac{d\bar{I}}{dz} = \overline{\overline{K}}_e \bar{I} + \int \overline{\overline{P}} \bar{I} d\Omega \tag{2}$$

where $\bar{I}$, $\overline{\overline{K}}_e$, and $\overline{\overline{P}}$ are the Stokes vector, extinction matrix and phase matrix of the medium, respectively. The phase matrix of the scatterers is written as shown below [1]:

$$\bar{P}\left(\theta, \emptyset; \theta', \emptyset'\right) = \langle |\Psi|^2 \rangle_n \cdot \overline{\overline{S}} = \begin{bmatrix} P_{vv} & P_{vh} \\ P_{hv} & P_{hh} \end{bmatrix} \tag{3}$$

where $\langle |\Psi|^2 \rangle_n$ is the dense medium phase correction factor that considers the coherency effect of closely spaced scatterers [8], and $\overline{\overline{S}}$ is the Stokes matrix as shown below [4]:

$$\overline{\overline{S}} = \frac{d^2\eta}{|E_o|^2} \text{Re} \begin{bmatrix} (E_v^s H_h^{s*})_{v\text{-}inc} & (E_v^s H_h^{s*})_{h\text{-}inc} \\ -(E_h^s H_v^{s*})_{v\text{-}inc} & -(E_h^s H_v^{s*})_{h\text{-}inc} \end{bmatrix} \tag{4}$$

where E_o is the amplitude of the incident field; d is the average distance between scatterers; E, H are the scattered electric and magnetic fields; v, h are the vertical and horizontal polarizations. For the proposed RT theoretical model, the Stokes matrix is represented by the scattering matrix of a scatterer of arbitrary shape computed with RHESA method. For spherical scatterers, Mie scattering formulation will be used.

The Stokes matrix of an arbitrary shape of scatterer was simulated using RHESA model. The scatterer to be simulated was first created in 3D geometry using a third party 3D modeling tool software such as ANSYS. Then the scatterer was divided into small groups using cubical box to form the lowest level of oct-tree. The benefit of using cubical box at the lowest level of oct-tree is because the scatterer can be divided into small groups without any overlapping. Each cube was then enclosed by a spherical equivalence surface (ES) to form the upper level of oct-tree without touching the internal primary sources. The upper layer of ESs becomes the parent group (ES^p) of the child group (ES^c) of ESs that form below it. An example of a rectangular scatterer is shown in Figure 3, and this process can be done for any arbitrary shape of scatterer.

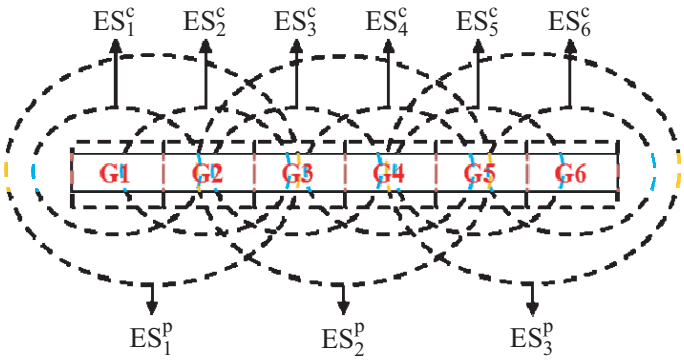

Figure 3. Construction of child groups (ES^c) and parent groups (ES^p) of equivalent sources using spherical equivalence surfaces.

To compute scattered fields using numerical technique, a popular way is to use MoM. Electric-field integral equation (EFIE) can be discretized and transformed into a matrix-form linear system with MoM. The formulation of unknown surface currents can then be written in a dense MoM matrix equation [19]:

$$\bar{Z} \cdot I = V \tag{5}$$

where $\bar{Z}$ is the impedance matrix, I the unknown coefficients vector, and V the excitation vector. Solving the above equation directly is difficult as it yields a large number of unknowns especially this involves volume integral equations (VIEs). With hierarchical form of ESs in RHESA model, the above equation can be rewritten into the form below [19]:

$$\bar{Z} \cdot I = \bar{Z}_{\text{near}} \cdot I + \bar{Z}_{\text{far}} \cdot I \tag{6}$$

RHESA divides Equation (5) into two categories of interactions which are near-field ($\bar{Z}_{\text{near}}$) and far-field ($\bar{Z}_{far}$) interactions as shown in Equation (6). The near-field interactions between groups can be computed directly through MoM while the far-field interactions between groups can be accelerated by equivalent source algorithm (ESA) before MoM is applied. This involves the following three steps: inside-out radiation, translation and outside-in radiation [19], as shown in Figure 4.

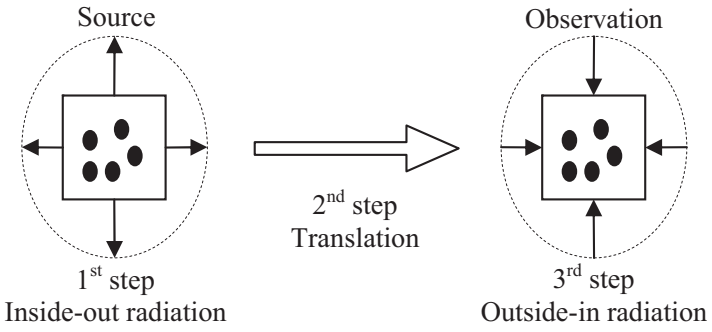

Figure 4. Far-field contributions from source group G^s to observation group G^o via ESA: inside-out radiation, translation and outside-in radiation. The spheres inside both groups represent the equivalent sources.

After breaking the scatterer into smaller groups and establishing the constructs of oct-tree, RHESA model performs the inside-out radiation from lower levels ESs to upper levels ESs at the source group G^s. At this step, the original sources that generate incident electric and magnetic fields are replaced by the equivalent sources on the ESs of the source group G^s by following the surface equivalence principle. The radiation of field of each level from child group to parent group is conducted using Stratton-Chu integral formulations. The same process also happens for outside-in radiation but in reverse direction.

Then at the second step, the far-field contributions from the equivalent sources of the source group G^s to the observation group G^o are computed through Stratton-Chu integral formulations. Lastly the third step is to perform the outside-in radiation from upper levels ESs to lower levels ESs in the observation group G^o. At this stage, the equivalent sources on the ES of the observation group G^o are updated with the radiated fields from the source group G^s which then generate the electric and magnetic fields inside the ES and the calculation of far-field contributions from group G^s to group G^o is completed [19].

With RHESA model, the scattered fields (E, H) in Equation (4) of arbitrary scatterer can be simulated, and the computed Stokes matrix using RHESA can be used in existing RT theoretical model. The design flow of overall model is shown in Figure 5 where in this case the Stokes matrix for Mie spherical scatterers can be replaced by the Stokes matrix calculated by RHESA for scatterers of arbitrary shapes.

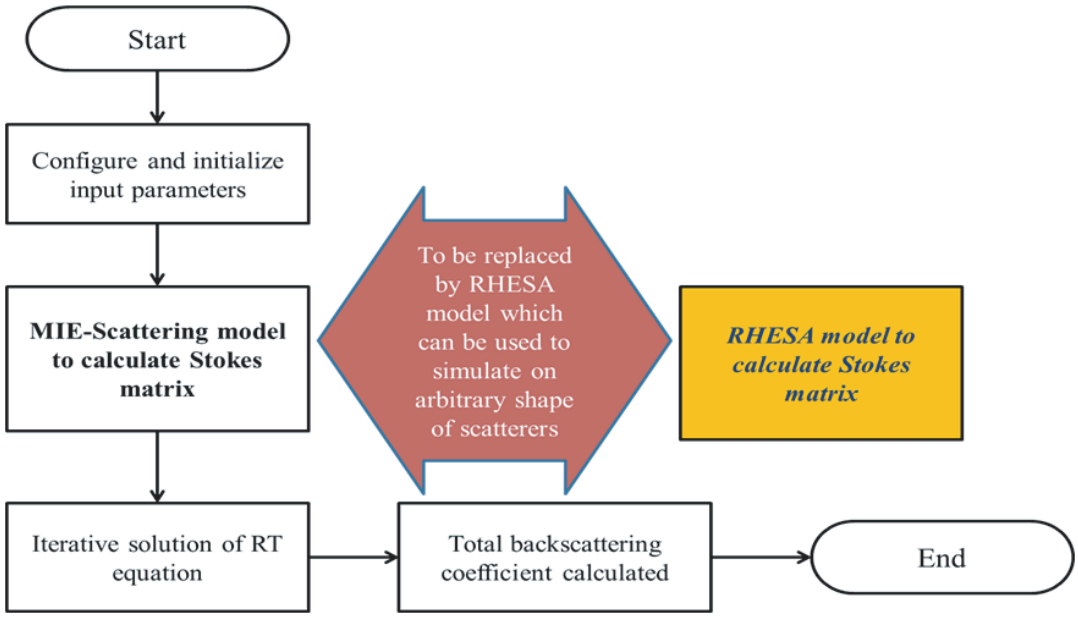

Figure 5. Overall design flow for the proposed RT theoretical model.

3. RESULTS AND ANALYSIS

Simulation results and validation of the proposed RT theoretical model with ground truth measurement data are presented in this section. The orientation of all shapes of scatterers were aligned to z direction (symmetry at z axis). As the shape of the particle selected for the simulations are all having an axis of symmetry, we can reduce the phase matrix to a simpler form [22] with faster computation. Each simulation only used one shape of scatterer and the scatterers were identical in size, relative permittivity and orientation with a distribution as explained in [2] and [8].

Figures 6(a) and (b) show the comparison among spherical shape, cylindrical shape and peanut shape against 7 different incidence angles for co-polarization and cross-polarization. The size of the cylinder used in the simulation was 0.35 mm radius and 1.7 mm length and the peanut shape of scatterers was actually a combination of two spherical scatterers of 0.45 mm radius each with the combined length of 1.36 mm. The radius of spherical scatterers was 0.55 mm. The dimensions of these shapes of scatterers were chosen so that the volumes of the three types of scatterers were about the same. The relative permittivity for the scatterers embedded in the air background medium was $3.15 + i0.001$ with a top layer of air ($1.0+i0.0$) and the lower half is soil ($6.0+i0.0$). Surface roughness for top surface was chosen to be 0.8 cm for rms-height and 6.0 cm for surface correlation length and those for bottom surface were 0.68 cm for rms-height and 6.0 cm for correlation length.

The co-polarization results show that the cylindrical shape can have higher total backscattering

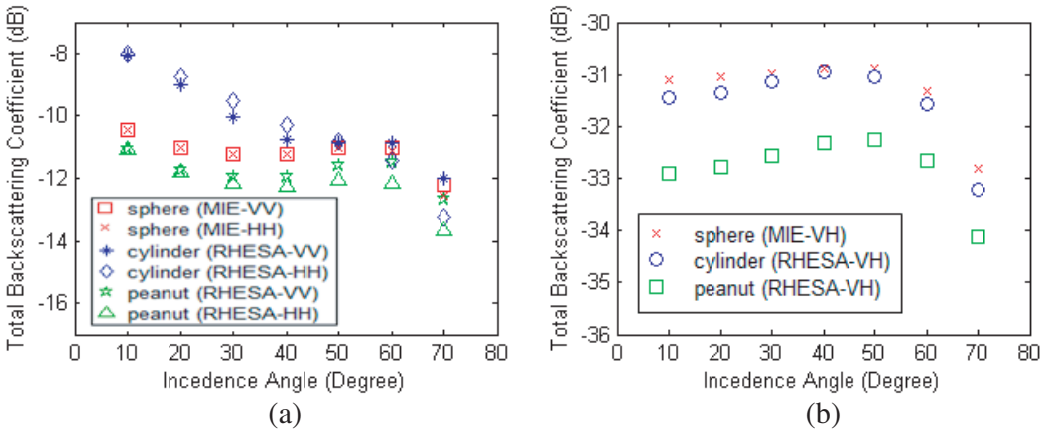

Figure 6. (a) Comparison among spherical shape, cylindrical shape and peanut shape against 7 different incidence angles at frequency 15.5 GHz for VV and HH polarization and (b) VH polarization.

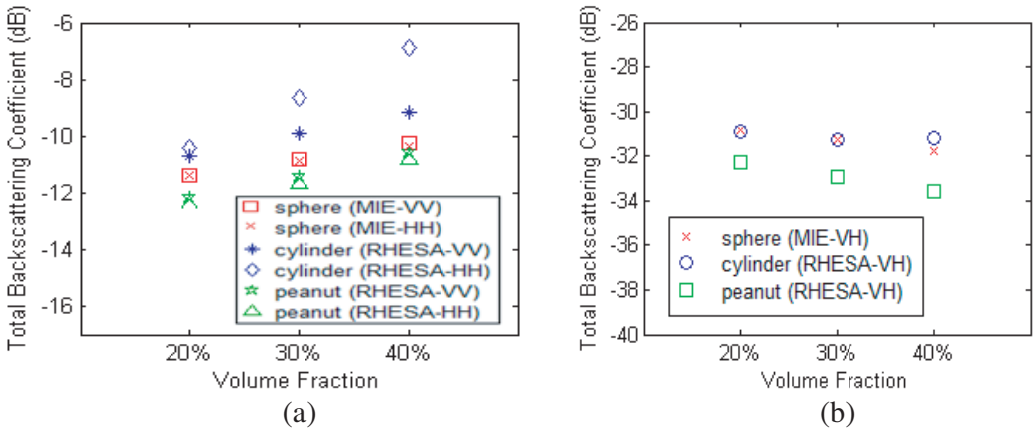

Figure 7. (a) Comparison among spherical shape, cylindrical shape and peanut shape against three different volume fractions (20%, 30% and 40%) at incidence angle $\theta = 35°$ at frequency 15.5 GHz for VV and HH polarization and (b) VH polarization.

coefficient than spherical and peanut shapes at lower incidence angles. On the other hand, for cross-polarization, peanut shape gives lower total backscattering coefficient than spherical and cylindrical shapes.

Figure 7 and Figure 8 show the comparison among spherical shape, cylindrical shape and peanut shape against three different volume fractions and layer thicknesses for co-polarization and cross-polarization. The sizes of the three types of scatterers were the same as those of Figure 6. Parameters used for the simulations are the same as those of Figure 6 except that the volume fraction and layer thickness are changed accordingly.

The following 4 graphs are comparisons of the new RT theoretical model with RHESA with ground truth measurement data collected from ice shelf areas [2] near Scott Base, Ross Island in Antarctica from 2002 to 2004 by RADARSAT satellite that operated at 5.3 GHz frequency (C-band) and NASA Cold Land Processes Field Experiment (CLPX) from 2002 to 2003 [23–25]. CLPX had conducted 4 Intensive Observation Periods (IOPs) during winter of 2002 and spring of 2003. For IOP1 and IOP3 these were carried out in February 2002 and February 2003. IOP2 and IOP4 were carried out in March 2002 and March 2003. The mentioned IOPs were conducted on the same day-of-year (DOY) schedule in order to maintain the consistency. During the IOPs, there were snow pits activities conducted within three larger-scale areas in northern Colorado (Fraser, North Park, and Rabbit Ears Meso-cell Study Areas

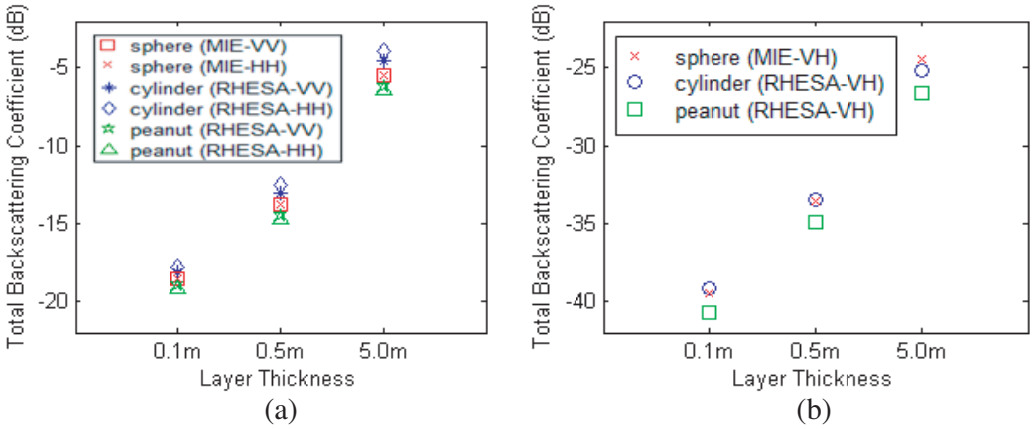

Figure 8. (a) Comparison among spherical shape, cylindrical shape and peanut shape against three different layer thicknesses (0.1 m, 0.5 m and 5.0 m) at incidence angle $\theta = 35°$ at frequency 15.5 GHz for VV and HH polarization and (b) VH polarization.

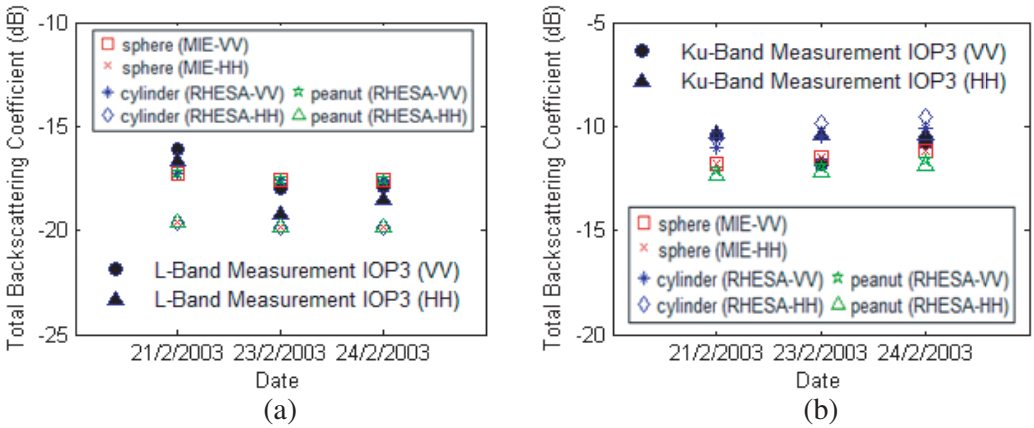

Figure 9. (a) Comparison of spherical shape, cylinder shape and peanut shape with data collected from CLPX during IOP3 at LSOS for VV and HH polarization at 35° incidence angle at L-band and (b) Ku-band.

(MSA)). Within these three larger-scale areas were three 1 km × 1 km intensive study areas (ISAs). Each ISA was divided into 4 sectors (Alpha, Beta, Charlie, and Delta) and there were 4 snow pit measurements performed within each sector. Within the Fraser MSA, there was the smallest study site (0.8 ha) called local scale observation site (LSOS). It was the most intensively measured location. The University of Michigan team set up a scatterometer, a radar system which could measure amplitude and phase of the backscattered signal to monitor the large clearing areas in LSOS. The system operated at two frequencies which were L-band (1.1–1.4 GHz) and Ku-band (15.25–15.75 GHz). The measurements were taken from three different incidence angles (20°, 35°, and 50°). Beside this, a Ku-band polarimetric scatterometer (POLSCAT) operating at 13.95 GHz was carried by an aircraft and the plane flew through the three MSA and generated the normalized radar cross section of the terrain.

As shown in Figure 9(a), 3 snow pit measurements of three different days sampled at LSOS during 2003 were selected to compare with the new RT theoretical model. Parameters measured during the IOP3 were snow depth, snow surface wetness, snow density, temperature, backscattered coefficient. 3 different shapes of scatterers were simulated for the L-band frequency. The lower half soil permittivity was estimated using the graph from [26]. The radius of spherical scatterers was 0.54 mm which was estimated based on the paper in [13]. The size of the cylinder used in the simulation was 0.35 mm radius and 1.7 mm length and the peanut shape of scatterers was actually a combination of two spherical

scatterers of 0.45 mm radius with the combined length of 1.36 mm. The volume of the three types of scatterers was kept as close as each other. All measurements from radar were taken at 35° incidence angle. The relative permittivity for scatterer was $3.15 + i0.001$ and the scatterers were embedded in the background medium of air, top layer was air $(1.0 + i0.0)$, and the lower half was soil $(6.0 + i0.0)$. Surface roughness for top surface was estimated based on the paper in [13] between range 0.6–0.8 cm for rms-height and 6.0–10.0 cm for surface correlation length, and those for bottom surface were 0.68–0.75 cm for rms-height and 6.0–10.0 cm for correlation length. The result shows that the simulated results match the ground truth measurement data.

Figure 9(b) shows the comparison using the same ground truth measurement data but at Ku-band frequency. At higher frequency, the shape of scatterers reflects noticeable difference among cylindrical shape, peanut shape and spherical shape. Simulation results for different shapes of scatterers were found to match with the ground truth measurement data and the cylindrical shape matched better for HH polarization at Ku-band. Beside this, the ground truth measurement data at Ku-Band shows that the HH polarization was higher than VV polarization. This was not reflected in the spherical scatterer simulation result but it was noticed from the simulation result of cylindrical scatterers.

As shown in Figure 10, 4 snow pit measurements locations, two from North Park's Illinois River during IOP1 and two from Rabbit Ears's Buffalo Pass and Spring Creek during IOP4 were selected to compare with the new RT theoretical model. The ground truth measurement data were from ISA located near to the flight lines (< 70 m) conducted during these periods and the POLSCAT scatterometer was carried onboard the plane. Sphere, cylinder and peanut shape of scatterers were used to run the simulation using the new RT theoretical model. Volume for these 3 different shapes of scatterers was kept as close as each other. The relative permittivity for the scatterers embedded in air background medium was $3.15 + i0.001$, the top layer was air $(1.0 + i0.0)$ and lower half was soil $(6.0 + i0.0)$. Surface roughness for top surface was estimated to be 0.6 cm for rms-height and 10.0 cm for surface correlation length and for bottom surface, it was 0.7–0.8 cm for rms-height and 10.0 cm for correlation length. At both IOP4 which had thicker snow layer (> 2 m) and higher volume fraction (> 36%) as compared with both IOP1 which had thinner snow layer (< 0.2 m) and lower volume fraction (< 26%), cylindrical shape gave quite high backscattering coefficient for HH polarization compared with spherical and peanut shape of scatterers and this could be because that the cylindrical shape is more sensitive to volume fraction as shown in Figure 7.

Figure 11 shows the comparison using 3 different shapes of scatterers which are peanut shape, cylindrical shape, and spherical shape with RADARSAT data from ice shelf sites in Antarctica [2] to see the impact on how different shapes of scatterers could contribute to the total backscattering coefficient.

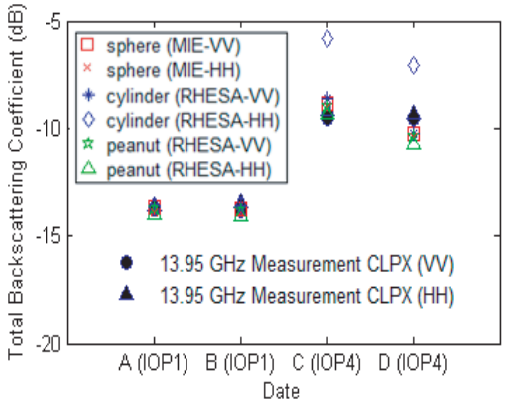

Figure 10. Comparison of spherical shape, cylindrical shape and peanut shape with data collected from CLPX during IOP1 (A, B) on 21/2/2002 and IOP4 (C, D) on 30/3/2003 for VV and HH polarization at 40° incidence angle at frequency of 13.95 GHz.

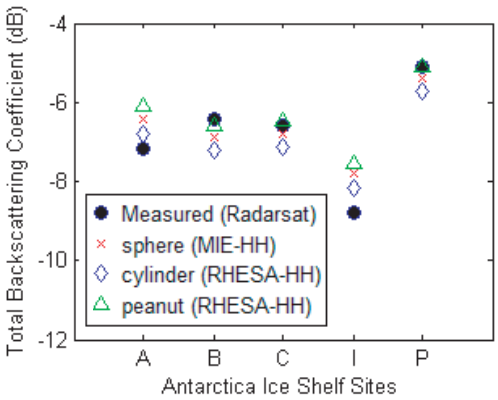

Figure 11. Comparison among five ice shelf sites A, B, C, I and P in Antarctica between 2002 and 2004 with 3 different shapes of scatterers which are peanut shape, cylindrical shape, and spherical shape for HH polarization at C-Band at 30° incidence angle.

The radius of spherical scatterers was 1.1 mm. The size of the cylinder used in the simulation was 1.1 mm radius and 1.47 mm length, and the peanut shape of scatterers was actually a combination of two spherical scatterers of 0.92 mm radius with the combined length of 2.77 mm. The volume of the three types of scatterers was kept as close as each other. At sites like B, C and P, the backscattering coefficients from scatterers of peanut shape match better than that of spherical shape and cylindrical shape. On the other hand, for sites A and I, cylindrical shape can match better than the others. The parameters used for simulations, such as relative permittivity of scatterer, surface roughness and layer thickness, were the same as those in paper [2] as same RADARSAT data and ground truth measurement data were used.

4. CONCLUSION

In this paper, a new RT theoretical model that incorporates RHESA model to give the capability to simulate arbitrary shape of scatterers has been developed and studied. Theoretical analysis with different incidence angles, volume fractions and layer thicknesses were performed. Comparisons with ground truth measurement data using new RT theoretical model were conducted. Results show that in some cases, non-spherical scatterers can have better match than spherical scatterers. This means that different shapes of scatterers could be important in contributions to total backscattering coefficient due to metamorphism and sintering process. With the new developed RT theoretical model with RHESA, future research works on different kinds of medium (such as vegetation) with irregular shapes of scatterers can be carried out.

ACKNOWLEDGMENT

This research work was financially supported by funding from the Asian Office of Aerospace R&D (AOARD) [Grant Number: FA2386-17-1-0010], Malaysia MOSTI Flagship Research Fund [Grant Number: FP1213E037-S2], Hong Kong GRF 17210815 and China NSFC 61271158.

REFERENCES

1. Syahali, S. and H. T. Ewe, "Remote sensing backscattering model for sea ice: Theoretical modelling and analysis," *Adv. Polar Sci.*, Vol. 24, No. 4, 248–257, 2013.
2. Albert, M. D., Y. J. Lee, H. T. Ewe, and H. T. Chuah, "Multilayer model formulation and analysis of radar backscattering from sea ice," *Progress In Electromagnetics Research*, Vol. 128, 267–290, 2012.
3. Tjuatja, S., A. K. Fung, and J. Bredow, "A scattering model for snow-covered sea ice," *IEEE Transactions on Geoscience and Remote Sensing*, Vol. 30, 804–810, 1992.
4. Fung, A. K., *Microwave Scattering and Emission Models and Their Applications*, Artech House, Norwood, MA, 1994.
5. Ewe, H. T. and H. T. Chuah, "Electromagnetic scattering from an electrically dense vegetation medium," *IEEE Transactions on Geoscience and Remote Sensing*, Vol. 38, No. 5, 2093–2105, 2000.
6. Karam, M. A., F. Amar, and A. K. Fung, "Electromagnetic wave scattering from a forest or vegetation canopy: Ongoing research at the University of Texas at Arlington," *IEEE Antennas and Propagation Magazine*, Vol. 35, No. 2, 18–26, Apr. 1993.
7. Ao, C. O. and J. A. Kong, "Analytical approximations in multiple scattering of electromagnetic waves by aligned dielectric spheroids," *J. Opt. Soc. Am. A*, Vol. 19, 1145–1156, Jun. 2002.
8. Chuah, H.-T., S. Tjuatja, A. K. Fung, and J. W. Bredow, "A phase matrix for a dense discrete random medium: evaluation of volume scattering coefficient," *IEEE Transactions on Geoscience and Remote Sensing*, Vol. 34, No. 5, 1137–1143, Sep. 1996.
9. Tsang, L., "Scattering of electromagnetic waves from a half space of nonspherical particles," *Radio Science*, Vol. 19, No. 06, 1450–1460, Nov.–Dec. 1984.

10. Wu, T. D., K. S. Chen, J. Shi, H. W. Lee, and A. K. Fung, "A study of an AIEM model for bistatic scattering from randomly rough surfaces," *IEEE Transactions on Geoscience and Remote Sensing*, Vol. 46, No. 9, 2584–2598, Sep. 2008.
11. Gherboudj, I., M. Bernier, F. Hicks, and R. Leconte, "Physical characterization of air inclusions in river ice," *Cold Reg. Sci. Technol.*, Vol. 49, No. 3, 179–194, Sep. 2007.
12. Gherboudj, I. and M. Bernier, "A backscatter modeling for river Ice: Analysis and numerical results," *IEEE Transactions on Geoscience and Remote Sensing*, Vol. 48, No. 4, Apr. 2010.
13. Du, J., J. Shi, and S. Wu, "A comparison of a second-order snow model with field observations," *Proceedings of IGRASS'05*, No. 05CH37663C, IEEE, Jul. 25–29, 2005.
14. Tsang, L., K. H. Ding, S. Huang, and X. Xu, "Electromagnetic computation in scattering of electromagnetic waves by random rough surface and dense media in microwave remote sensing of land surfaces," *Proceedings of the IEEE*, Vol. 101, No. 2, 255–279, Feb. 2013.
15. Colbeck, S. C., "A review of sintering in seasonal snow," *CRREL Report 97-10*, 11, 1997.
16. Gibson, W. C., *The Method of Moments in Electromagnetics*, Taylor & Francis Group, LLC, 2008.
17. Li, M. K. and W. C. Chew, "Wave-field interaction with complex structures using equivalence principle algorithm," *IEEE Transactions on Antennas and Propagation*, Vol. 55, No. 1, 130–138, Jan. 2007.
18. Yla-Oijala, P. and M. Taskinen, "Solving electromagnetic scattering by multiple targets with surface equivalence principle algorithm," *2009 3rd European Conference on Antennas and Propagation*, 88–92, Berlin, 2009.
19. Fu, X., L. J. Jiang, and H. T. Ewe, "A novel relaxed hierarchical equivalent source algorithm (RHESA) for electromagnetic scattering analysis of dielectric objects," *Journal of Electromagnetic Waves and Applications*, Vol. 30, No. 12, 1631–1642, 2016.
20. Lu, C. C. and W. C. Chew, "A multilevel algorithm for solving a boundary integral equation of wave scattering," *Micr. Opt. Technol. Lett.*, Vol. 8, 466–70, 1994.
21. Taflove, A. and S. C. Hagness, "Computational electrodynamics: The finite-difference time-domain method," 2nd Edition, Artech House, Boston, MA, 2000.
22. Mishchenko, M. I., A. A. Lacis, and L. D. Travis, *Scattering, Absorption, and Emission of Light by Small Particles*, Cambridge University Press, 2002.
23. Hardy, J., J. Pomeroy, T. Link, D. Marks, D. Cline, K. Elder, and R. Davis, *CLPX-Ground: Snow Measurements at the Local Scale Observation Site (LSOS)*, IOP3, NSIDC DAAC, Boulder, Colorado, USA, 2003.
24. Sarabandi, K., *CLPX-Ground: Ground-based L and Ku Band Polarimetric Scatterometry, Version 1*, IOP3, NSIDC DAAC, Boulder, Colorado, USA, 2003.
25. Yueh, S. H., *CLPX-Airborne: Polarimetric Ku-band Scatterometer (POLSCAT) Data*, IOP1 & IOP4, NSIDC DAAC, Boulder, Colorado, USA, 2003.
26. Zhang, L., J. Shi, Z. Zhang, and K. Zhao, "The estimation of dielectric constant of frozen soil-water mixture at microwave bands," *Proceedings of 2003 IEEE International Geoscience and Remote Sensing Symposium*, Vol. 4, 2903–2905, 2003.